# Xk-Related Protein 8 and CED-8 Promote Phosphatidylserine Exposure in Apoptotic Cells

Jun Suzuki,[1] Daniel P. Denning,[2] Eiichi Imanishi,[1] H. Robert Horvitz,[2] Shigekazu Nagata[1,3]*

A classic feature of apoptotic cells is the cell-surface exposure of phosphatidylserine (PtdSer) as an "eat me" signal for engulfment. We show that the Xk-family protein Xkr8 mediates PtdSer exposure in response to apoptotic stimuli. Mouse *Xkr8*$^{-/-}$ cells or human cancer cells in which Xkr8 expression was repressed by hypermethylation failed to expose PtdSer during apoptosis and were inefficiently engulfed by phagocytes. Xkr8 was activated directly by caspases and required a caspase-3 cleavage site for its function. CED-8, the only *Caenorhabditis elegans* Xk-family homolog, also promoted apoptotic PtdSer exposure and cell-corpse engulfment. Thus, Xk-family proteins have evolutionarily conserved roles in promoting the phagocytosis of dying cells by altering the phospholipid distribution in the plasma membrane.

Phospholipids are distributed asymmetrically between the outer and inner leaflets of plasma membranes (*1*): Phosphatidylserine (PtdSer) and phosphatidylethanolamine (PtdEtn) localize exclusively to the inner leaflet, whereas 60 to 70% of phosphatidylcholine (PtdCho) and sphingomyelin (SM) are found on the outer leaflet. This asymmetric distribution is disrupted during apoptosis, and exposed PtdSer on dying cells serves as an "eat me" signal to facilitate phagocytosis (*2*, *3*). PtdSer exposure and the more general transfer of phospholipids between the inner and outer leaflets are probably mediated by phospholipid scramblases (*1*), the identities of which are disputed (*4*).

We previously generated a mouse Ba/F3 pro-B cell line (Ba/F3-PS19) with a high level of PtdSer exposure, constructed a cDNA library (of clones >2.5 kb), and discovered TMEM16F, a transmembrane protein required for $Ca^{2+}$-dependent phospholipid scrambling but not apoptosis-dependent PtdSer exposure (*5*, *6*). To identify molecules that mediate apoptotic PtdSer exposure, we introduced a Ba/F3-PS19 cDNA library (of clones 1.0 to 2.5 kb) into Ba/F3 cells, serially enriched for cells with high PtdSer exposure, and established a cell line (LD-PS5-2-2) with a high level of PtdSer exposure (Fig. 1A) (see supplementary materials and methods). LD-PS5-2-2 cells carried a cDNA encoding Xkr8, a member of the evolutionarily conserved XK protein family (*7*) (figs. S1 and S2). With the use of the programs Transmembrane Prediction (www.ch.embnet.org) and Transmembrane Hidden Markov Model (www.cbs.dtu.dk), analyses of the amino acid sequences of vertebrate Xkr8 orthologs suggested that Xkr8 contains six transmembrane regions flanked by cytosolic N and C termini (fig. S3).

We transformed mouse T cell lymphoma WR19L cells with Fas (*8*) (WR-Fas). Fas ligand (FasL) efficiently induced apoptosis of the WR-Fas cells, accompanied by caspase-3 activation and PtdSer exposure (Fig. 1B and fig. S4). The introduction of mouse Xkr8-GFP [mXkr8 fused to green fluorescent protein (GFP)], but not mTMEM16F-GFP, increased the fraction of PtdSer-exposing cells generated by FasL (Fig. 1B). The expression of m*Xkr8* short hairpin RNAs (shRNAs) in WR-Fas cells decreased the amount of the endogenous m*Xkr8* mRNA by 76 to 82% (fig. S5) and the fraction of cells with FasL-induced PdtSer-exposure (Fig. 1C), but not levels of caspase-3 activation (fig. S5). The transformation of m*Xkr8* shRNA-expressing cells with human (h)*Xkr8* cDNA, which is not recognized by the m*Xkr8* shRNAs, restored FasL-induced PdtSer exposure. hXkr8-GFP expressed in human 293T cells localized primarily to the plasma membrane (Fig. 1D), suggesting that Xkr8 functions at the cell surface to promote apoptotic PtdSer exposure.

Human PLB-985 leukemia and Raji lymphoma cells do not expose PtdSer during apoptosis (*9*, *10*). Studies using real-time reverse transcription polymerase chain reaction (RT-PCR) indicated that the amount of *Xkr8* mRNA in PLB-985 and Raji cells was 8 and 9%, respectively, of those in Namalwa cells (Fig. 2A). PLB-985 or Raji cell transformants expressing hXkr8 responded to apoptotic stimuli by exposing PtdSer (Fig. 2B). PtdSer exposure is necessary for the recognition of apoptotic cells by phagocytes

[1]Department of Medical Chemistry, Graduate School of Medicine, Kyoto University, Yoshida-Konoe, Sakyo-ku, Kyoto, Kyoto 606-8501, Japan. [2]Howard Hughes Medical Institute and Department of Biology, Massachusetts Institute of Technology, Cambridge, MA 02139, USA. [3]Core Research for Evolutional Science and Technology, Japan Science and Technology Corporation, Yoshida-Konoe, Sakyo, Kyoto 606-8501, Japan.

*Corresponding author. E-mail: snagata@mfour.med.kyoto-u.ac.jp

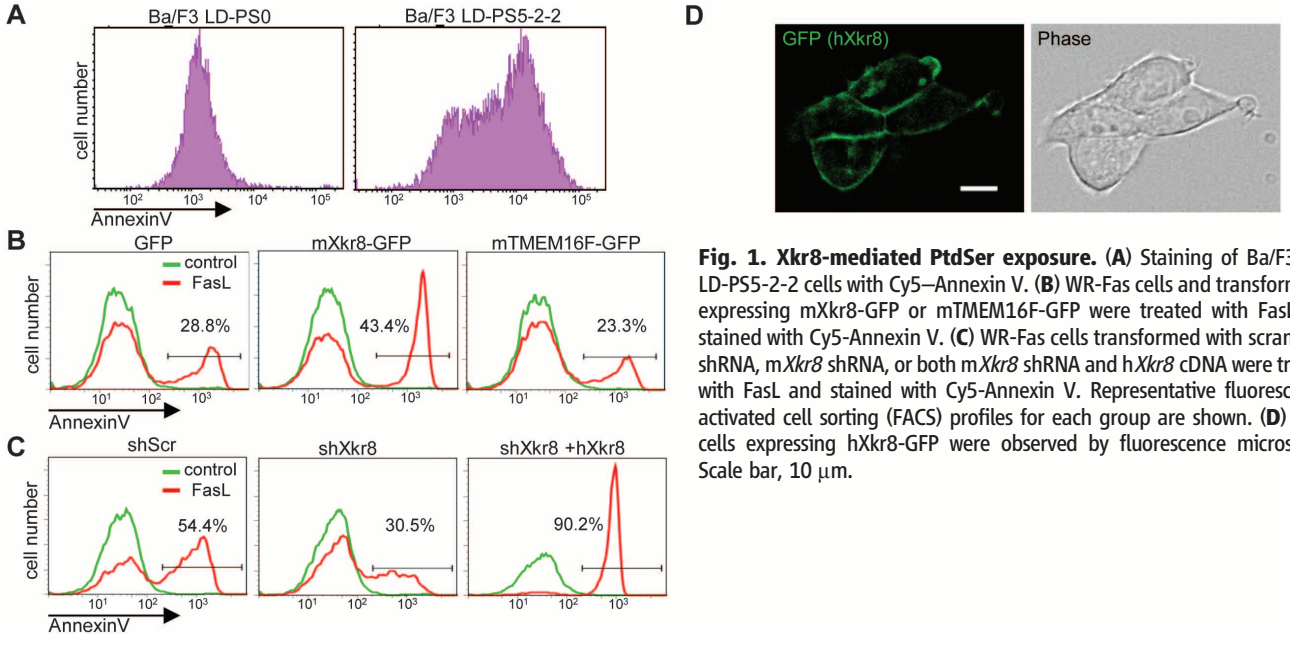


**Fig. 1. Xkr8-mediated PtdSer exposure.** (**A**) Staining of Ba/F3 and LD-PS5-2-2 cells with Cy5–Annexin V. (**B**) WR-Fas cells and transformants expressing mXkr8-GFP or mTMEM16F-GFP were treated with FasL and stained with Cy5-Annexin V. (**C**) WR-Fas cells transformed with scrambled shRNA, m*Xkr8* shRNA, or both m*Xkr8* shRNA and h*Xkr8* cDNA were treated with FasL and stained with Cy5-Annexin V. Representative fluorescence-activated cell sorting (FACS) profiles for each group are shown. (**D**) 293T cells expressing hXkr8-GFP were observed by fluorescence microscopy. Scale bar, 10 μm.

(*3*, *10*, *11*). Accordingly, whereas apoptotic PLB-985 cells were rarely engulfed by macrophages, their Xkr8 transformants were frequently internalized (Fig. 2C). Caspase-3 activation, DNA fragmentation, cell death, and cell shrinkage occurred similarly in PLB-985 cells with or without Xkr8 expression, indicating that Xkr8 and PtdSer exposure had no obvious effects on other aspects of the apoptotic process (fig. S6). The program CpG Island Searcher (http://cpgislands.usc.edu) identified two CpG islands near the transcription start site of the h*Xkr8* gene (fig. S7). Bisulfite DNA sequencing (*12*) indicated that none of the 23 CpGs between –232 and +4 of the h*Xkr8* gene was methylated in peripheral blood leukocyte, Jurkat, or Namalwa cells (fig. S7). By contrast, these CpGs were methylated with more than 90% probability in PLB-985 and Raji cells. Treatment of PLB-985 cells with 5-aza-2′-deoxycytidine (DAC) increased *Xkr8* mRNA levels (Fig. 2D). After 7 days of DAC treatment, all CpGs were demethylated (fig. S7), and *Xkr8* mRNA levels were 91% of that in Namalwa cells. Accordingly, DAC-treated PLB-985 cells exposed PtdSer upon ultraviolet (UV) irradiation (Fig. 2E). We suggest that the methylation of CpG islands in the *Xkr8* promoter in PLB-985 and Raji cells blocks *Xkr8* gene expression and prevents apoptotic PtdSer exposure.

We used RO09-0198 to assay staurosporine-treated, Xkr8-expressing PLB-985 cells for PtdEtn exposure, and we used 1-oleoyl-2-{6-[(7-nitro-2-1,3-benzoxadiazol-4-yl)amino]hexanoyl}-sn-glycero-3-phosphocholine (NBD-PC) and NBD-sphingosine-1-phosphocholine (NBD-SM) to assay for PtdCho and SM internalization, respectively. Inhibitor of caspase-activated DNase (ICAD) was cleaved equally well in PLB-985 and its hXkr8 transformants after staurosporine treatment (fig. S8). By contrast, apoptotic hXkr8-expressing cells (but not parental cells) stained with RO09-0198 and internalized NBD-PC and NBD-SM (fig. S8), indicating that Xkr8, like TMEM16F (*5*), promotes the scrambling of multiple lipid species. Unlike TMEM16F, Xkr8 had no effect on the $Ca^{2+}$-induced exposure of PtdSer (fig. S9), suggesting that distinct pathways control $Ca^{2+}$-induced phospholipid scrambling and apoptosis-induced scrambling. These findings are consistent with reports that B cell lines from Scott syndrome patients, who carry a null mutation in *TMEM16F*, respond to apoptotic stimuli by exposing PtdSer (*13*), and that mouse *Bak*$^{-/-}$*Bax*$^{-/-}$ platelets, which do not undergo apoptosis, expose PtdSer upon $Ca^{2+}$ ionophore treatment (*14*).

We used the program CASVM (www.casbase.org) to analyze Xkr8 sequences from six vertebrates and, thus, identify a conserved caspase-3–recognition site near the Xkr8 C terminus (fig. S1). We generated a mutant version of hXkr8 (2DA) in which the putative caspase-recognition sequence at position 355 was changed from PDQVDG to PAQVAG (P, Pro; D, Asp; Q, Gln; V, Val; G, Gly; A, Ala) (fig. S3). PLB-985 cells expressing wild-type (WT) hXkr8-GFP exposed PtdSer in response to staurosporine (Fig. 3A), accompanied by the loss of a 52-kD hXkr8-GFP band on polyacrylamide gels and the appearance of a 29-kD band detected with antibodies to GFP (anti-GFP) (Fig. 3B). After staurosporine treatment, hXkr8(2DA)-GFP failed to promote PtdSer exposure and was not proteolytically processed; ICAD was cleaved in cells expressing either the WT or 2DA mutant of hXkr8, indicating similar caspase-3 activity in both cell lines. Processing of mXkr8-GFP at the caspase-recognition site during apoptosis was also observed in WR-Fas cells after treatment with FasL (Fig. 3C). The solubilized membrane fraction from cells expressing hXkr8-GFP was then incubated with human caspases. Western blot analysis with anti-GFP showed that caspases-3 and -7 cleaved the WT but not 2DA mutant hXkr8 (Fig. 3D). Thus, mammalian Xkr8 is activated to expose PtdSer via caspase-mediated cleavage of its cytosolic C terminus.

Mouse *Xkr8* mRNA was detectable in most mouse tissues (fig. S10), with notably high expression in the testes. We established m*Xkr8*-conditional knockout mice (fig. S11), from which we prepared mouse embryonic fibroblasts (MEFs). After treatment with staurosporine, *Xkr8*$^{+/-}$ but not *Xkr8*$^{-/-}$ MEFs exposed PtdSer (Fig. 4A). Similarly, *Xkr8*$^{flox/flox}$ and *TMEM16F*$^{-/-}$ but not *Xkr8*$^{-/-}$ fetal thymocyte (IFET) cell lines exposed PtdSer in response to FasL (Fig. 4B), although caspase-3 was activated similarly in these cell lines (fig. S12). The transformation of *Xkr8*$^{-/-}$ IFETs with mXkr8 restored PtdSer exposure in response to FasL.

The protein CED-8 is the only *Caenorhabditis elegans* homolog of Xk proteins and was previously shown to control the timing of programmed cell deaths (*15*) (fig. S2). To determine if CED-8 (like Xkr8) promotes phagocytosis, we examined *ced-8* eggs for "floater" cells, which are generated in embryos defective in engulfment; floaters are a subset of apoptotic cells that, if not engulfed (e.g., in *ced-1*, *-2*, *-5*, *-6*, *-7*, *-10*, or *-12* mutants), detach from the embryo (Fig. 4C and fig. S13) (*16*, *17*). *ced-8* eggs contained floaters, and *ced-8* mutations synergistically enhanced the number of floaters in mutants partially defective in engulfment.

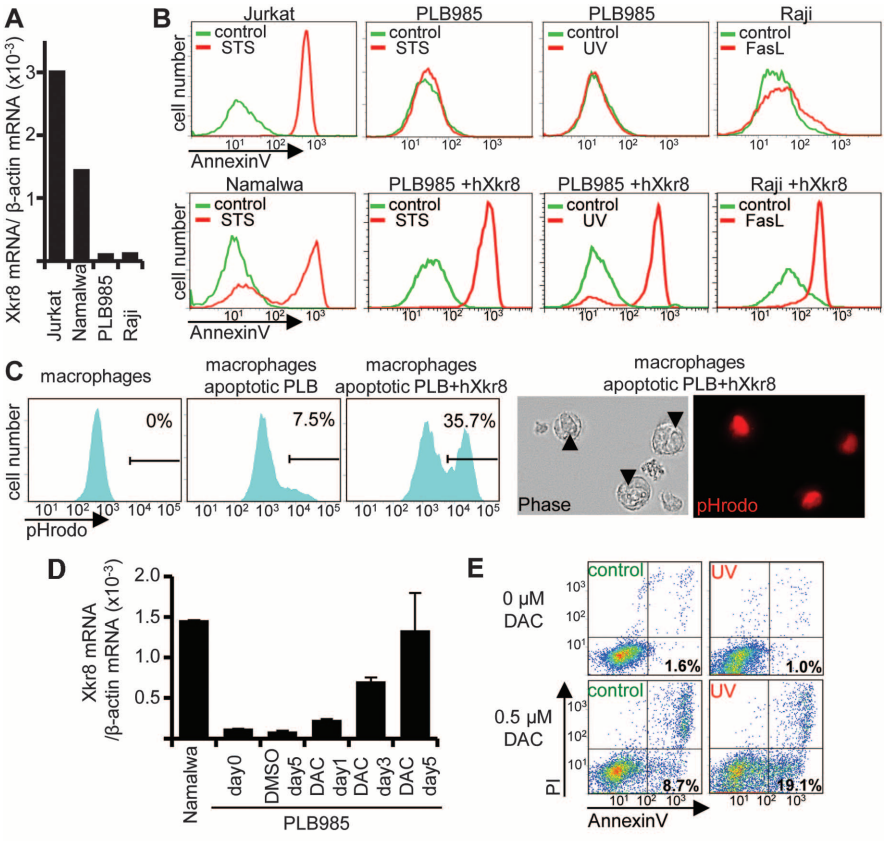


**Fig. 2. Epigenetic repression of Xkr8 in human cancer cell lines.** (**A**) Abundance of h*Xkr8* mRNA relative to β-*actin* mRNA was determined by real-time RT-PCR. (**B**) The indicated cell lines and hXkr8 transformants were treated with apoptotic stimuli and stained with Cy5–Annexin V. STS, staurosporine. (**C**) PLB-985 cells and hXkr8 transformants were treated with UV, labeled with pHrodo, and incubated with CD11b$^{+}$ peritoneal macrophages. (Left) FACS profiles for pHrodo-positive CD11b$^{+}$ cells are shown, as is the average percentage of pHrodo$^{+}$ cells from three experiments. (Right) Macrophages (arrowheads) engulfing apoptotic cell were observed by fluorescence microscopy. (**D**) PLB-985 cells were treated with DAC, and *Xkr8* mRNA was quantified relative to *GADPH* mRNA by real-time RT-PCR. DMSO, dimethyl sulfoxide. (**E**) PLB-985 cells were treated with DAC for 5 days, exposed to UV, and stained with Cy5–Annexin V and propidium iodide.

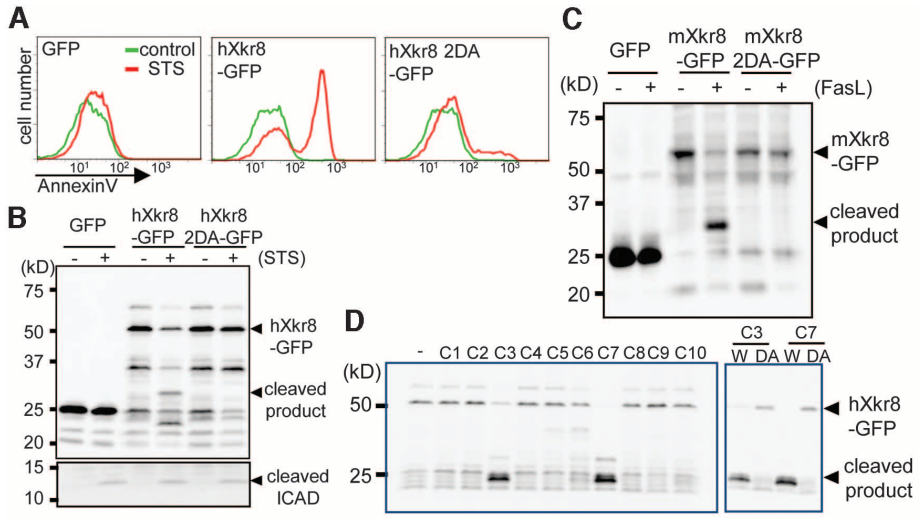


**Fig. 3. Activation of Xkr8 by caspase cleavage.** (**A** and **B**) PLB-985 and transformants expressing hXkr8-GFP or hXkr8 2DA-GFP were treated with STS and stained with Cy5–Annexin V (A). In (B), the cell lysates were analyzed by Western blotting with anti-GFP and anti-ICAD antibodies. (**C**) WR-Fas and transformants expressing GFP, mXkr8-GFP, or mXkr8 2DA-GFP were treated with FasL. Cell lysates were analyzed by Western blotting with anti-GFP. (**D**) The membrane fraction of PLB-985 cells expressing hXkr8-GFP (W) or the 2DA mutant (DA) was incubated with human caspases (C1 to C10, caspase-1 to caspase-10) and analyzed by Western blotting with anti-GFP antibody.

This enhancement was dependent on the caspase gene *ced-3* (fig. S14), which is required for apoptosis. The PtdSer-binding protein MFG-e8::Venus (*18*) associated with 94% of apoptotic cell corpses in the ventral cords of WT animals, but only with 21% of those in *ced-8* mutants (Fig. 4D). Similarly, PtdSer was exposed on newly detached floaters from *ced-1* but not *ced-8* or *ced-1*; *ced-8* embryos (fig. S15). Because 21% of *ced-8* ventral cord cell corpses had normal PtdSer exposure, additional factors probably contribute to this process.

In short, the Xk-related proteins Xkr8 and CED-8 promote caspase-dependent PtdSer exposure during apoptosis. Based on the following observations, Xkr8 and CED-8 probably act at a late step in PtdSer exposure, possibly in phospholipid scrambling: (i) *Xkr8*-deficient cells expose PtdSer in response to $Ca^{2+}$, indicating that Xkr8 is dispensable for steps before PtdSer exposure, including PtdSer biogenesis and localization; (ii) Xkr8 is directly activated by caspase cleavage, suggesting Xkr8 does not function before the onset of apoptosis; and (iii) Xkr8 and CED-8 are transmembrane proteins at the plasma membrane and, therefore, are positioned to effect, or interact with partners that effect, the externalization of PtdSer during apoptosis.

**Fig. 4. Promotion of PtdSer exposure and cell-corpse engulfment by mouse Xkr8 and *C. elegans* CED-8.** (**A**) MEFs from *Xkr8*$^{+/-}$ and *Xkr8*$^{-/-}$ embryos were treated with STS or control buffer for 8 hours and stained with Cy5–Annexin V. (**B**) IFETs of the indicated genotypes were treated with FasL and stained with Cy5–Annexin V and PI. (**C**) The number of floater cells per egg (n) was counted for each genotype. Error bars indicate SD. ***$P < 0.0001$ in a Student's $t$ test for each pairwise comparison between *ced-x* and *ced-8*; *ced-x* double mutants. (**D**) PtdSer was detected using MFG-e8::Venus. Shown is the cell corpse of P12.aap (arrowhead), which undergoes apoptosis and is engulfed by P12.pa (arrow). The death of P12.aap is accompanied by PtdSer exposure in WT but not in *ced-8* (*n1891*) animals. In addition, P12.pa, like other *C. elegans* engulfing cells (*23*, *24*), exposes PtdSer on its outer plasma membrane during engulfment. DIC, differential interference contrast microscopy.

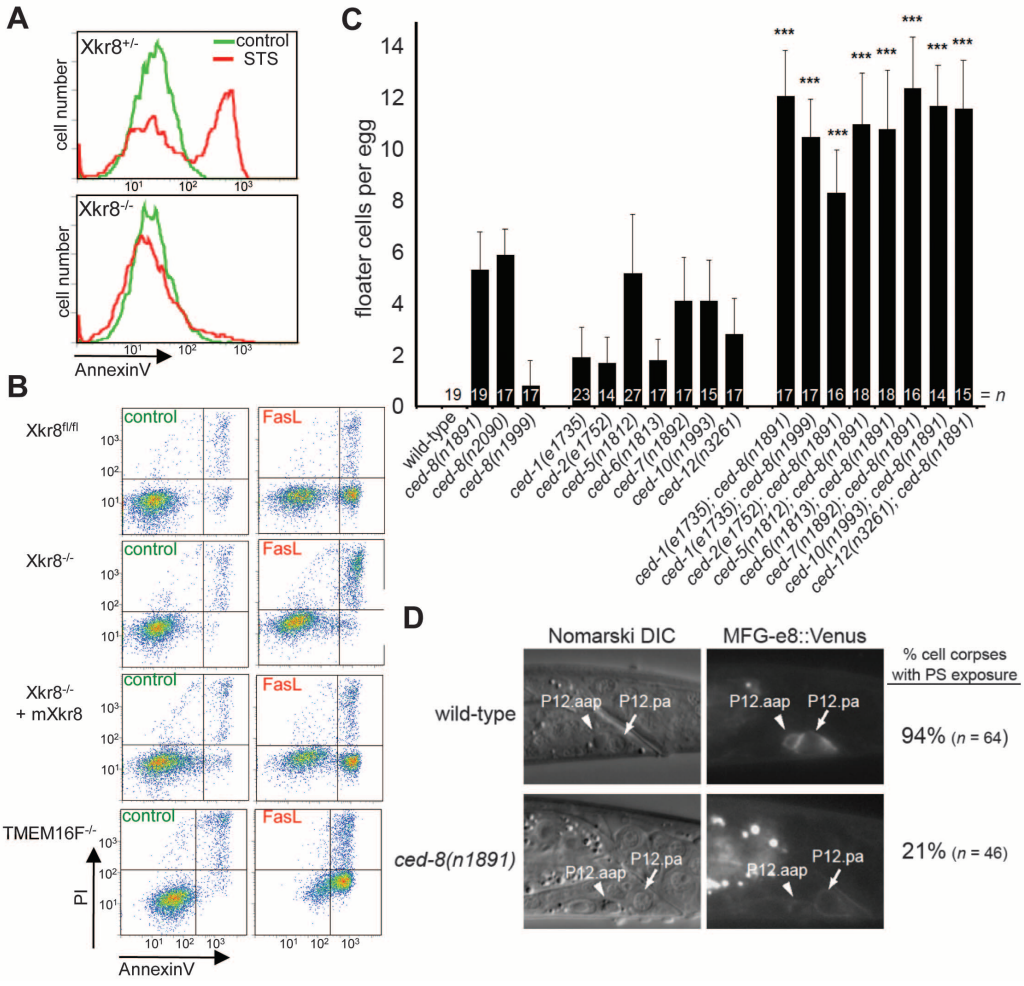

Although intracellular concentrations of $Ca^{2+}$ increase during apoptosis (*19*, *20*), the involvement of $Ca^{2+}$ in apoptotic PtdSer exposure is unclear (*4*), and our observations do not support a generalization. We found that FasL-induced PtdSer exposure was $Ca^{2+}$-dependent in WR19L cells, but not Ba/F3 cells, and that when WR19L cells were transformed with Xkr8, they lost the $Ca^{2+}$ requirement for the apoptotic exposure of PtdSer. These results, together with the constitutive activity of overexpressed Xkr8 in Ba/F3 but not other cells, suggest that Xkr8 might cooperate with $Ca^{2+}$-regulated proteins in some cell-specific contexts.

The swift clearance of dead cells is essential for maintaining homeostasis, and the masking of PtdSer on apoptotic cells or the failure of the engulfment system can cause autoimmune disorders like systemic lupus erythematosus (*3*, *21*). Our finding that Xkr8 is epigenetically repressed in cancer cells suggests a mechanistic link among inflammation, autoimmunity, and cancer (*22*).

### References and Notes


1. P. A. Leventis, S. Grinstein, *Annu. Rev. Biophys.* **39**, 407–427 (2010).
2. K. S. Ravichandran, U. Lorenz, *Nat. Rev. Immunol.* **7**, 964–974 (2007).
3. S. Nagata, R. Hanayama, K. Kawane, *Cell* **140**, 619–630 (2010).
4. E. M. Bevers, P. L. Williamson, *FEBS Lett.* **584**, 2724–2730 (2010).
5. J. Suzuki, M. Umeda, P. J. Sims, S. Nagata, *Nature* **468**, 834–838 (2010).
6. J. Suzuki *et al.*, *J. Biol. Chem.* **288**, 13305–13316 (2013).
7. G. Calenda *et al.*, *Gene* **370**, 6–16 (2006).
8. S. Nagata, *Cell* **88**, 355–365 (1997).
9. B. Fadeel *et al.*, *Biochem. Biophys. Res. Commun.* **266**, 504–511 (1999).
10. V. A. Fadok, A. de Cathelineau, D. L. Daleke, P. M. Henson, D. L. Bratton, *J. Biol. Chem.* **276**, 1071–1077 (2001).
11. R. Hanayama *et al.*, *Nature* **417**, 182–187 (2002).
12. J. G. Herman, J. R. Graff, S. Myöhänen, B. D. Nelkin S. B. Baylin, *Proc. Natl. Acad. Sci. U.S.A.* **93**, 9821–9826 (1996).
13. P. Williamson *et al.*, *Biochemistry* **40**, 8065–8072 (2001).
14. S. M. Schoenwaelder *et al.*, *Blood* **114**, 663–666 (2009).
15. G. M. Stanfield, H. R. Horvitz, *Mol. Cell* **5**, 423–433 (2000).
16. Y.-C. Wu, G. M. Stanfield, H. R. Horvitz, *Genes Dev.* **14**, 536–548 (2000).
17. D. P. Denning, V. Hatch, H. R. Horvitz, *Nature* **488**, 226–230 (2012).
18. V. Venegas, Z. Zhou, *Mol. Biol. Cell* **18**, 3180–3192 (2007).
19. D. L. Bratton *et al.*, *J. Biol. Chem.* **272**, 26159–26165 (1997).
20. M. B. Hampton, D. M. Vanags, M. I. Pörn-Ares, S. Orrenius, *FEBS Lett.* **399**, 277–282 (1996).
21. L. E. Muñoz, K. Lauber, M. Schiller, A. A. Manfredi, M. Herrmann, *Nat. Rev. Rheumatol.* **6**, 280–289 (2010).
22. A. L. Franks, J. E. Slansky, *Anticancer Res.* **32**, 1119–1136 (2012).
23. J. Mapes *et al.*, *Curr. Biol.* **22**, 1267–1275 (2012).
24. Y. Zhang, H. Wang, E. Kage-Nakadai, S. Mitani, X. Wang, *Curr. Biol.* **22**, 1276–1284 (2012).



**Acknowledgments:** We thank W. Hiraoka, M. Umeda, and M. Fujii for the PLB-985 cell line, the RO09-0198 peptide, and secretarial assistance, respectively. This work was supported in part by Grants-in-Aid for Specially Promoted Research from the Japan Society for the Promotion of Science (JSPS) to S.N., a Grant-in-Aid for Young Scientists (B) from JSPS to J.S., and postdoctoral fellowships from the Damon Runyon Cancer Research Foundation and the Charles A. King Trust to D.P.D. H.R.H. is the David H. Koch Professor of Biology at the Massachusetts Institute of Technology and is a Howard Hughes Medical Institute Investigator.


### Supplementary Materials

www.sciencemag.org/cgi/content/full/science.1236758/DC1
Materials and Methods
Figs. S1 to S15
References (*25*–*44*)


19 February 2013; accepted 26 June 2013
Published online 11 July 2013;
10.1126/science.1236758


# Reprogramming of Intestinal Glucose Metabolism and Glycemic Control in Rats After Gastric Bypass


**Nima Saeidi,[1,2,3]* Luca Meoli,[1]* Eirini Nestoridi,[1]* Nitin K. Gupta,[1] Stephanie Kvas,[1] John Kucharczyk,[1] Ali A. Bonab,[2] Alan J. Fischman,[2] Martin L. Yarmush,[2,3] Nicholas Stylopoulos[1]†**



**The resolution of type 2 diabetes after Roux-en-Y gastric bypass (RYGB) attests to the important role of the gastrointestinal tract in glucose homeostasis. Previous studies in RYGB-treated rats have shown that the Roux limb displays hyperplasia and hypertrophy. Here, we report that the Roux limb of RYGB-treated rats exhibits reprogramming of intestinal glucose metabolism to meet its increased bioenergetic demands; glucose transporter-1 is up-regulated, basolateral glucose uptake is enhanced, aerobic glycolysis is augmented, and glucose is directed toward metabolic pathways that support tissue growth. We show that reprogramming of intestinal glucose metabolism is triggered by the exposure of the Roux limb to undigested nutrients. We demonstrate by positron emission tomography–computed tomography scanning and biodistribution analysis using 2-deoxy-2-[18F]fluoro-D-glucose that reprogramming of intestinal glucose metabolism renders the intestine a major tissue for glucose disposal, contributing to the improvement in glycemic control after RYGB.**


Roux-en-Y gastric bypass (RYGB) induces substantial and sustained weight loss and is a highly effective treatment for severe obesity (*1*–*3*). The results of three recent prospective studies suggest that RYGB is the best treatment option for obesity-related diabetes (*4*–*6*). Interestingly, the improvement in glucose homeostasis occurs early after the RYGB procedure, before any appreciable weight loss, and patients are often able to discontinue their antidiabetic medications before hospital discharge (*4*, *5*, *7*, *8*). The precise mechanisms underlying the resolution of diabetes after RYGB have not been determined (*3*, *8*–*10*).

Several studies in rodents and one study in humans have previously described that the Roux limb displays morphological changes, characterized by hypertrophy and hyperplasia after RYGB (*11*–*16*). However, the importance of the morphological adaptation of the Roux limb, in itself, in the metabolic effects of RYGB remains largely unknown. Because the construction of the Roux limb is one of the fundamental components of the RYGB procedure (Fig. 1A) (*17*, *18*), we hypothesized that the beneficial effect of RYGB on glucose homeostasis may stem from changes in the metabolism within this reconfigured jejunal segment to meet the increased bioenergetic demands of tissue growth and maintenance, possibly in response to its exposure to undigested nutrients. To study the Roux limb, we performed RYGB in rats (*19*). RYGB led to substantial and sustained weight loss and improvement in glucose metabolism in diet-induced obese (DIO) rats, recapitulating the effects observed in humans (fig. S1, A to E). RYGB also improved glycemic control in two nonobese, diabetic rodent models with impaired insulin secretion: streptozotocin (STZ)–induced diabetic and Goto-Kakizaki (GK) rats (Fig. 1, B to D, and fig. S1, F to I). We also observed intestinal remodeling, characterized by increased intestinal mass due to hyperplasia and hypertrophy, in the Roux limb of RYGB-treated rats (figs. S2 to S4 and supplementary text 1).

To test our hypothesis, we initially sought to identify possible metabolic changes in the Roux limb of RYGB-treated rats. We compared its metabolic profile with the profile of corresponding segments of the jejunum of sham-operated rats, using a quantitative polar metabolomic profiling platform. The metabolomic profiling showed increased concentrations of glucose-6-phosphate, d-gluconate, 6-phospho-d-gluconate and nicotinamide adenine dinucleotide phosphate ($NADP^+$) in the Roux limb, suggesting that the oxidative phase of the pentose phosphate pathway (PPP) is stimulated (fig. S5, A and B, and table S1). The changes in the metabolites of the nonoxidative phase of the PPP did not reach statistical significance,


[1]Center for Basic and Translational Obesity Research, Division of Endocrinology, Boston Children's Hospital, Harvard Medical School, Boston, MA 02115, USA. [2]Shriners Hospital for Children, Boston, MA 02114, USA. [3]Center for Engineering in Medicine, Massachusetts General Hospital, Harvard Medical School, Boston, MA 02114, USA.

*These authors contributed equally to this work.
†Corresponding author. E-mail: Nicholas.Stylopoulos@childrens.harvard.edu